Received: 6 December 2020 | Accepted: 3 June 2021 | Published online: 27 August 2021

DOI: 10.1002/saj2.20289

Soil Science Society of America Journal

SOIL PHYSICS & HYDROLOGY

New model for estimating geometric tortuosity of variably saturated porous media using 3D synchrotron microcomputed tomography imaging

Zaher A. Jarrar[1] | **Riyadh I. Al-Raoush**[2] | **Jamal A. Hannun**[2] | **Khalid A. Alshibli**[1]

[1] Dep. of Civil & Env. Engineering, 325 John Tickle Building, Univ. of Tennessee, Knoxville, TN 37996, USA

[2] Dep. of Civil and Architectural Engineering, Qatar Univ., Doha PO Box 2713, Qatar

Correspondence
Riyadh I. Al-Raoush, Dep. of Civil and Architectural Engineering, Qatar Univ., PO Box 2713, Doha, Qatar.
Email: riyadh@qu.edu.qa

Assigned to Associate Editor Xinhua Jia.

Abstract

Tortuosity has a significant impact on flow and transport characteristics of porous media and plays a major role in many applications such as enhanced oil recovery, contaminant transport in aquifers, and fuel cells. Most analytical and theoretical models for determining tortuosity have been developed for ideal systems with assumptions that might not be representative of natural porous media. In this paper, geometric tortuosity was directly determined from three-dimensional (3D) tomography images of natural unconsolidated sand packs with a wide range of porosity, saturation, grain size distribution, and morphology. One hundred and thirty natural unconsolidated sand packs were imaged using 3D monochromatic and pink-beam synchrotron microcomputed tomography imaging. Geometric tortuosity was directly determined from the 3D images using the centroids of the connected paths in the flow direction of the media, and multivariate nonlinear regression analysis was adopted to develop a simple practical model to predict tortuosity of variably saturated natural unconsolidated porous media. Wetting phase saturation was found to provide a good estimate of relative tortuosity with an R^2 value of .93, even with a porosity variation between 0.3 and 0.5 of the porous media systems. The proposed regression model was compared to theoretical and analytical models available in the literature and was found to provide better estimates of geometric tortuosity with an R^2 value of .9 and a RMSE value of 0.117.

1 | INTRODUCTION

Fluid transport in porous media can be encountered in a wide range of applications, including enhanced oil recovery, groundwater flow, contaminant transport in aquifers, geological storage of CO_2, fuel cells, and batteries. Tortuosity of transport paths in the pore space has a profound impact on the transport and flow characteristics of porous media. Pore space tortuosity affects electrical conductivity (Garrouch et al., 2001; Weerts et al., 2001), permeability (Duda et al., 2011; Vervoort & Cattle, 2003), diffusion (Gao et al., 2014; Grathwohl, 2012), thermal conductivity (Qin et al., 2019; Xu et al., 2018), fluid entrapment (Androutsopoulos & Salmas, 2000; Salmas & Androutsopoulos, 2001), and acoustics properties (Li & Payandeh, 2016; Zielinski, 2012) of porous media. Tortuosity has been categorized in the literature into four main classes: geometric, diffusive, hydraulic,

Abbreviations: 2D, two-dimensional; 3D, three-dimensional; CT, X-ray computed tomography; SMT, synchrotron microcomputed tomography; SMT-M, monochromatic synchrotron microcomputed tomography; SMT-P, pink beam synchrotron microcomputed tomography.

and electric. Geometric tortuosity (τ) is defined as the ratio of the average length of the geometrical paths through the porous medium to the straight line length across the medium (Clennell, 1997). Diffusive tortuosity (τ_d) is defined as the square of the ratio of the average length of a chemical's diffusive pathway to the straight line length (Epstein, 1989). Clennell (1997) defined hydraulic tortuosity (τ_h) as the square of the ratio of the flux-weighted average path length for hydraulic flow to the straight-line length. Electric tortuosity (τ_e) is defined as the square of the ratio of the average path length for electrical flow to the straight line length (Wong, 1999). More information about different types of tortuosity are referred to in the critical review conducted by Ghanbarian, Hunt, Ewing, et al. (2013).

Whereas many theoretical, analytical, and experimental approaches have been reported in the literature to model tortuosity in porous media, the focus of this study is the geometric tortuosity. Lanfrey et al. (2010) developed a theoretical tortuosity model for a fixed-bed of randomly packed mono-sized particles:

$$\tau = 1.23\left[\frac{(1-\phi)^{4/3}}{I_R^2\phi}\right] \quad (1)$$

where ϕ is the porosity, and I_R is the roundness shape factor for a given particle defined as

$$I_R = \frac{\sqrt[3]{36\pi V_p^2}}{S_p} \quad (2)$$

where V_p and S_p are the volume and surface area of the particle, respectively. By definition, $S_p = 1$ for spheres and is less than unity for nonspherical particles. The model is based on the assumption that the sinuous channels, which represent the tortuous paths, have a constant proportionality of 0.84 between the cross sectional area and the square of hydraulic diameter. Pisani (2011) derived a simple expression of tortuosity as a function of porosity by numerical simulation of diffusion processes in porous media composed of spherical particles as

$$\tau = 1 + 0.64(1-\phi) \quad (3)$$

Additional analytical tortuosity models from the literature are presented in Table 1 where these models were derived for fully saturated or dry porous media systems. Moreover, previous analytical and theoretical models determine tortuosity for ideal systems with underlying assumptions that might not be representative of natural porous material.

Ghanbarian, Hunt, Sahimi, et al. (2013) developed a geometric tortuosity model applicable to variably saturated porous media based on percolation theory and finite-size scaling approach:

$$\tau = \left[\frac{\theta - \theta_t + (C/L_s)^{\frac{1}{\nu}}}{1-\theta_t}\right]^{\nu - \nu D_x} \quad (8)$$

where ν is a scaling component that equals 4/3 in two dimensions (2D) and 0.88 in 3D, D_x is the fractal dimensionality of the optimal paths (1.21 in 2D and 1.43 in 3D) or backbone cluster (value depends on the percolation model), C is the typical throat length in the porous media, which can be determined from the pore-throat length distribution mode, L_s is the system size, θ is the volumetric water content, and θ_t is the critical volumetric water content for percolation, which is

Core Ideas

- Geometric tortuosity was directly determined for 130 natural porous media.
- A model was developed to predict saturated and unsaturated geometric tortuosity.
- The proposed model accounts for porosity, saturation, and morphology of particles.

TABLE 1 Additional analytical tortuosity models from the literature

Equation no.	Type	Model	Description	Reference
4	Hydraulic	$\tau = \frac{\phi}{1-(1-\phi)^{\frac{2}{3}}}$	Idealized granular pore microstructure	Du Plessis and Masliyah (1991)
5	Geometric	$\tau = \frac{1}{2}\left[1 + \frac{1}{2}\sqrt{1-\phi} + \frac{\sqrt{(\sqrt{1-\phi}-1)^2 + \frac{1-\phi}{4}}}{1-\sqrt{1-\phi}}\right]$	Two-dimensional porous media composed of square particles	Yu and Li (2004)
6	Hydraulic	$\tau = \sqrt{\frac{2\phi}{3[1-1.209(1-\phi)^{\frac{2}{3}}]} + \frac{1}{3}}$	Used a volume averaging concept to express tortuosity of mono-sized spherical arrays	Ahmadi et al. (2011)
7	Geometric	$\tau = (\frac{19}{18})^{\ln(\phi)/\ln(\frac{8}{9})}$	Tortuosity of flow paths in Sierpinski carpet	Li and Yu (2011)

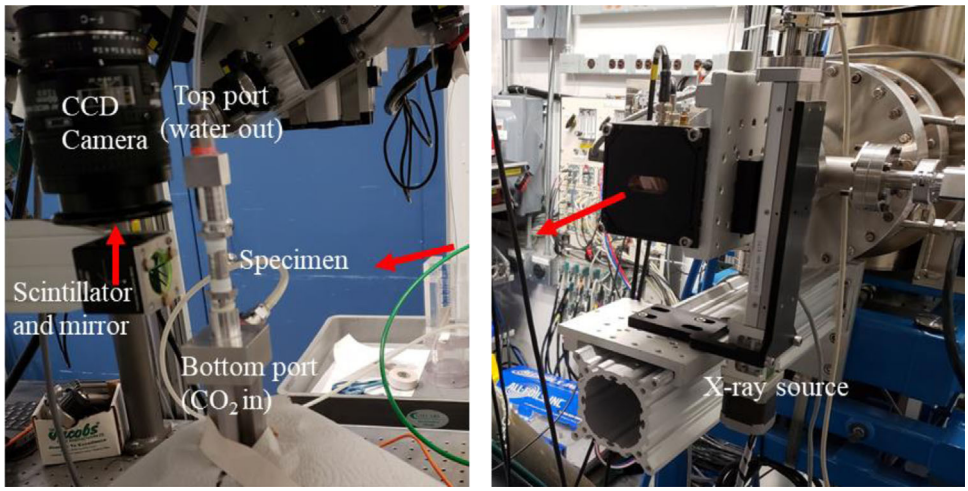

FIGURE 1 Experimental setup at Beamline 13D, Advanced Photon Source, Argonne National Laboratory. CCD, charge-coupled device

TABLE 2 Summary of the physical properties of the 130 porous media systems used to determine geometric tortuosity

Sample	ϕ	D_{50}	I_R	I_{sph}	C_u	C_c	S	No. of saturation levels	Image size	Image resolution
	%	μm					%		voxels	μm voxel^{-1}
1	45.8	525	0.77	1.76	1.51	1.08	72.0–100	4	1,920 × 1,920 × 1,200	4.92
2	47.2	426	0.78	1.72	1.33	1.02	83.3–100	6		
3	46.6	421	0.78	1.70	1.31	1.03	83.1–100	5		
4	43.8	431	0.76	1.63	1.40	1.08	71.4–100	8		
5	50.4	368	0.76	1.48	1.39	1.06	67.0–100	9		
6	44.3	368	0.78	1.55	1.30	1.01	71.3–100	9		
7	45.6	392	0.70	1.31	1.57	1.12	59.4–100	12		
8	39.9	411	0.76	1.59	2.05	1.02	43.5–100	10		
9	39.5	443	0.76	1.58	2.36	1.10	34.7–100	10		
10	39.3	412	0.75	1.57	2.20	1.09	42.0–100	10		
11	35.0	626	0.86	1.71	2.76	1.03	74.7–100	4	400 × 400 × 400	11.22
12	34.0	602	0.87	1.70	2.66	1.00	39.8–100	6		
13	34.7	608	0.87	1.73	2.66	1.02	31.0–100	15		
14	35.2	596	0.88	1.72	1.46	1.11	13.5–100	9		
15	33.3	796	0.91	1.72	1.17	0.97	100	1	550 × 550 × 520	11.22
16	35.6	511	0.87	1.64	1.26	0.98	100	1		
17	37.2	516	0.69	1.22	1.65	0.98	100	1		
18	33.2	539	0.87	1.58	1.37	0.98	100	1		
19	30.4	572	0.85	1.50	1.54	0.99	100	1		
20	36.5	652	0.89	1.58	1.23	0.99	100	1		
21	47.5	959	0.74	1.82	1.36	0.97	100	1		
22	48.3	618	0.69	1.29	1.60	0.90	100	1		
23	48.9	690	0.55	0.93	2.10	1.02	100	1		
24	45.8	673	0.71	1.35	1.82	0.90	100	1		
25	48.2	722	0.67	1.24	1.91	1.01	100	1		
26	43.5	776	0.74	1.54	1.39	0.96	100	1		
27	39.6	712	0.82	1.56	1.31	0.99	100	1		

Note. ϕ, porosity; D_{50}, median grain diameter; I_R, roundness index; I_{sph}, sphericity index; C_u, uniformity coefficient; C_c, coefficient of curvature; S, degree of saturation.

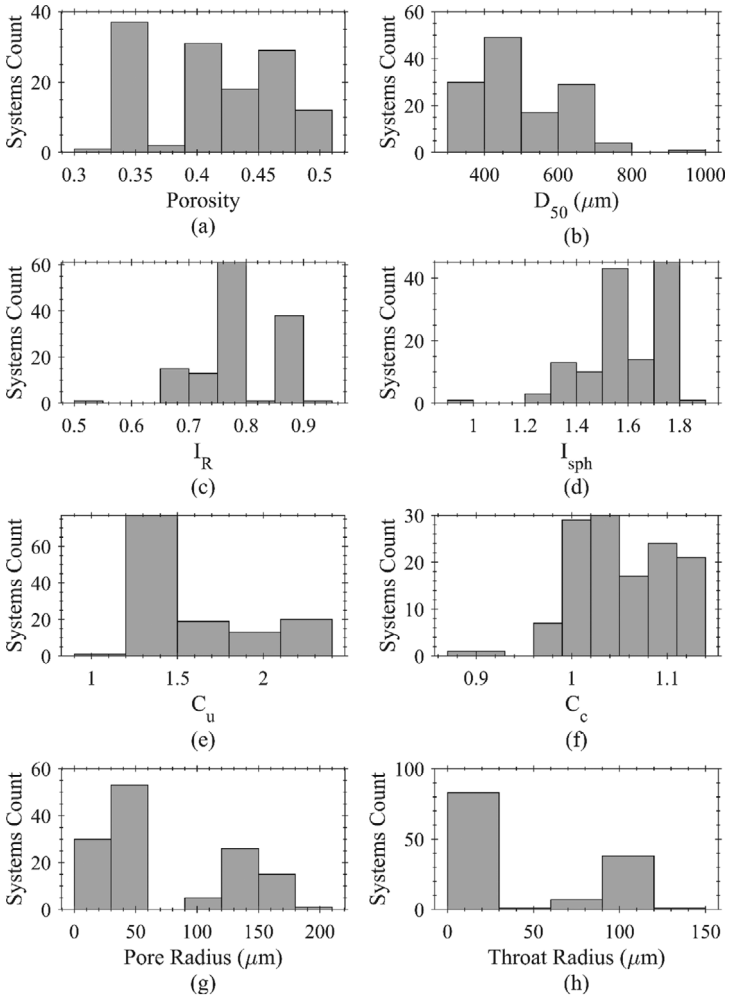

FIGURE 2 Histograms of (a) porosity, (b) median grain diameter (D_{50}), (c) roundness index (I_R), (d) sphericity index (I_{sph}), (e) uniformity coefficient (C_u), (f) coefficient of curvature (C_c), (g) mean pore radius, and (h) mean throat radius of the 130 systems reported in this study

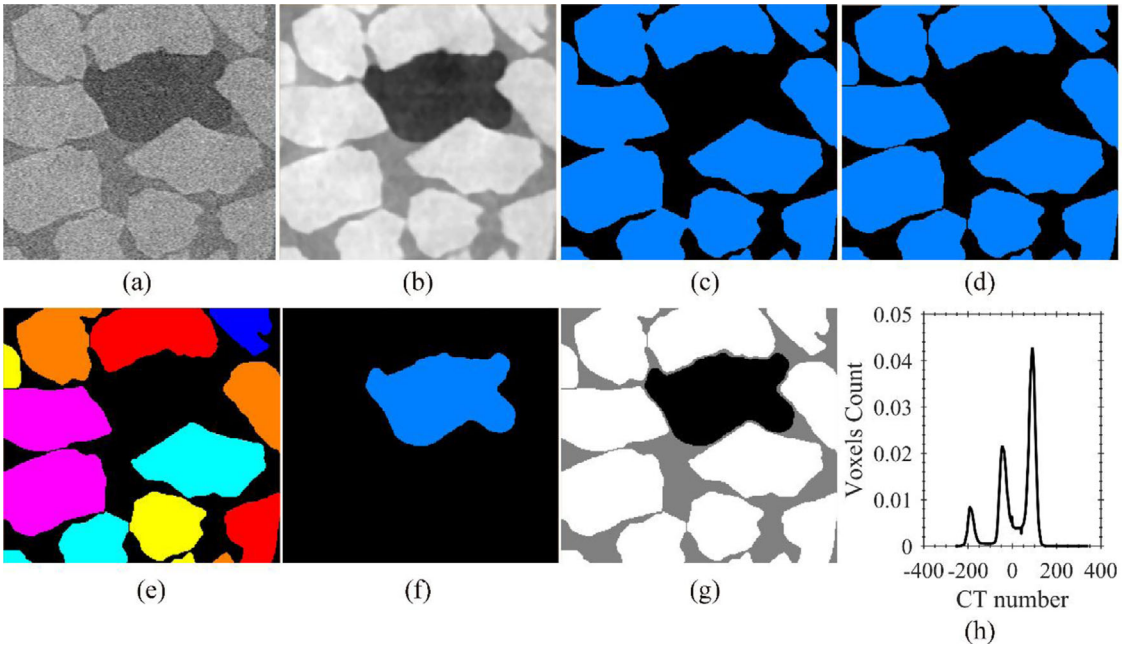

FIGURE 3 Image processing steps on a zoomed view of an XY slice of a sample system: (a) raw image, (b) filtered image, (c) binarized sand image, (d) binarized sand separated image, (e) sand labeled image, (f) binarized nonwetting phase image, (g) three-phase segmented image (gas is black, water is gray, and sand is white), and (h) histogram of the filtered image. CT, computed tomography

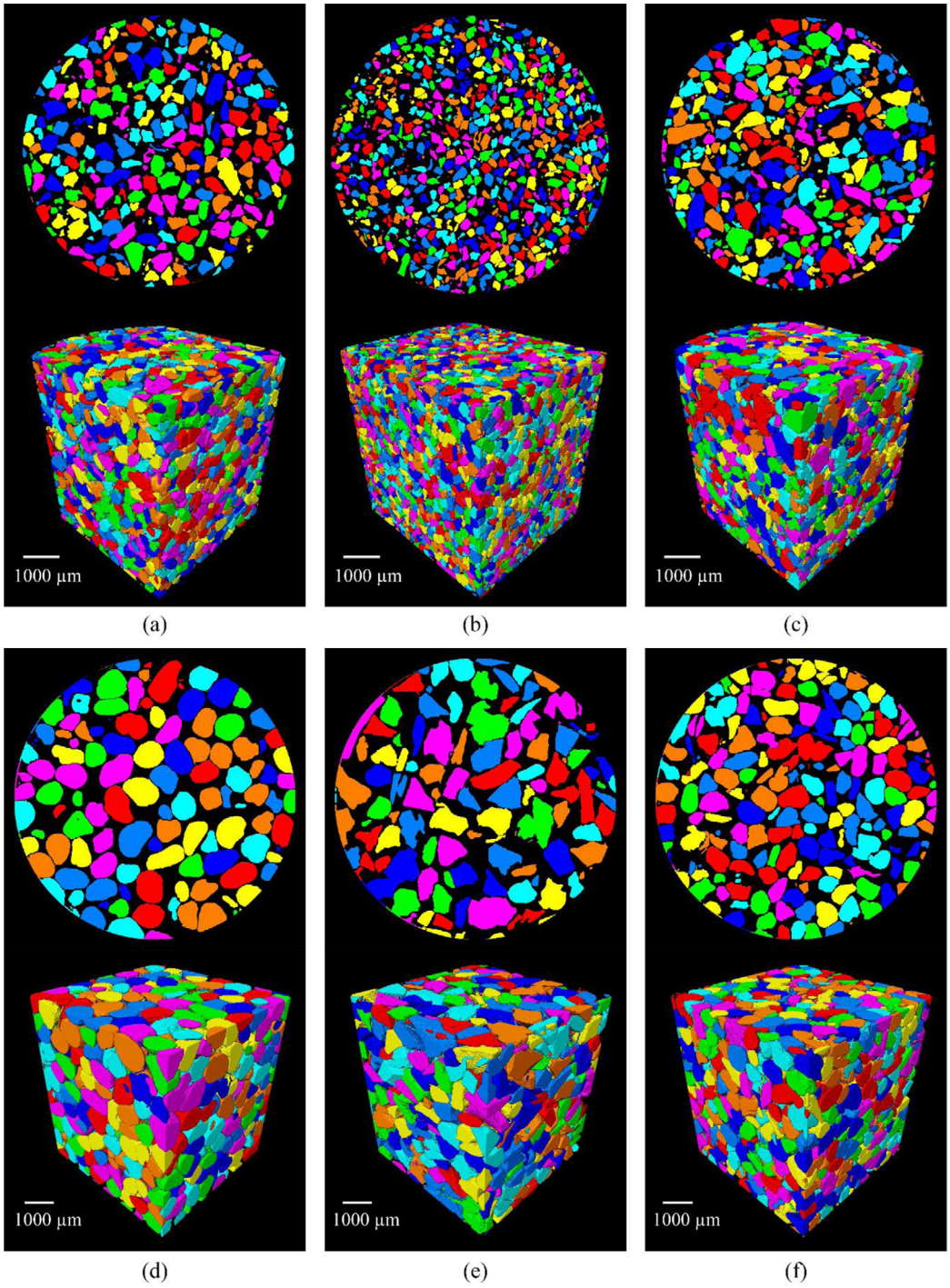

FIGURE 4 Two-dimensional cross-section and volume rendering snapshots for selected labeled images from (a) Sample 1, (b) Sample 5, (c) Sample 8, (d) Sample 15, (e) Sample 21, and (f) Sample 27

the minimum water content required for the existence of a system-spanning cluster of interconnected water-filled pores. (Ghanbarian, Hunt, Sahimi, et al., 2013) defined the relative tortuosity (τ_r) as the ratio of geometrical tortuosity in an unsaturated (i.e., partially saturated) medium to the geometrical tortuosity of the same medium at full saturation, τ_s:

$$\tau_r = \frac{\tau}{\tau_s} = \left[\frac{\theta - \theta_t + \left(C/L_s\right)^{\frac{1}{\nu}}}{\phi - \theta_t + \left(C/L_s\right)^{\frac{1}{\nu}}}\right]^{\nu - \nu D_x} \quad (9)$$

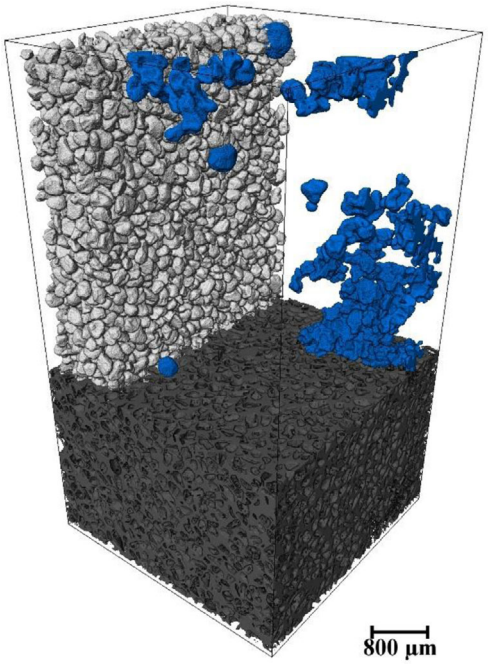

FIGURE 5 Volume rendering image for a sample system depicting the three segmented phases; sand is light gray, water is dark gray, and gas is blue

Tortuosity has been measured experimentally indirectly by conducting fluid diffusion experiments (Corrochano et al., 2015; Soukup et al., 2015) and electrical conductivity measurements (Morin et al., 2010). For instance, Iversen and Jørgensen (1993) determined tracer diffusion coefficients of SO_4^{2-} and CH_4 in different types of sediments including sandy sediments and fine-grained silt and clay to estimate tortuosity as

$$\tau = \sqrt{1 + 2(1 - \phi)} \tag{10}$$

Comiti and Renaud (1989) proposed the following equation to estimate tortuosity based on permeability measurements for polyvinyl chloride (PVC) platy particles and glass spheres as

$$\tau = 1 - p \ln(\phi) \tag{11}$$

where p is a fitting parameter which depends on the shape of particles and was reported by Mauret and Renaud (1997) to be 0.49 for the case of spherical particles. Although these experimental methods provide a fair estimate of tortuosity, they fail to relate the estimated tortuosity to the geometry and topology of the pore space.

Recent advances in nondestructive imaging techniques such as X-ray computed tomography (CT) motivated researchers to investigate the complex pore structure of porous media. Several algorithms were reported in the literature to measure geometric tortuosity using 3D volume images. Such algorithms include medial axis (Al-Raoush & Madhoun, 2017; Takahashi et al., 2009), Dijkstra algorithm (Pardo-Alonso et al., 2014), random walk simulation (Promentilla et al., 2016), chessboard distance algorithm (FEI, 2018), and thin-line skeleton (Rotger et al., 2003). Available commercial software use different algorithms for measuring tortuosity from 3D CT images. For instance, the medial axis algorithm is used in 3DMA software (Jung et al., 2014; Takahashi et al., 2015) and 3DMA-Rock software (Naveed et al., 2013; Neethirajan et al., 2008), whereas the chessboard distance algorithm is used in Avizo software (FEI, 2018). Naveed et al. (2013) used 3DMA-Rock software to estimate tortuosity of 10 natural porous media specimens with different shapes and mean particle diameters and reported that geometric tortuosity can be estimated as

$$\tau = 0.19 d_{50} + 1.45 \tag{12}$$

where d_{50} is the mean particle diameter in mm. However, the main limitation of the model defined by Equation 12 is the limited number of samples used to generate the model and the exclusion of the influence of porosity in the model.

As observed from previous studies, analytical and theoretical models that determine geometric tortuosity were developed for ideal systems with underlying assumptions that might not be representative of natural porous media. Moreover, synergies of wetting phase saturation and geometric characteristics of the natural porous media on geometric tortuosity were not explicitly presented. Therefore, the objective of this study was to develop a physically realistic model to predict geometric tortuosity of porous media as a function of porosity, wetting phase saturation, coefficient of curvature, and roundness of the porous media grains. Additionally, the proposed model was compared with analytical and theoretical models reported in the literature. One hundred and thirty samples of natural unconsolidated sand packs with a wide range of porosity, saturation, grain size distribution, and morphology porous media were imaged using 3D monochromatic and pink-beam synchrotron microcomputed tomography imaging. Geometric tortuosity was directly determined from 3D images.

2 | MATERIALS AND METHODS

2.1 | 3D SMT

3D synchrotron microcomputed tomography (SMT) is an enhancement to industrial CT where a synchrotron radiation source is used to produce a high-intensity X-ray beam. Typical SMT imaging uses a monochromator (SMT-M) to produce a monochromatic x-ray beam with tunable energy allowing for element-specific imaging and reducing beam hardening artifacts (Kinney & Nichols, 1992). However,

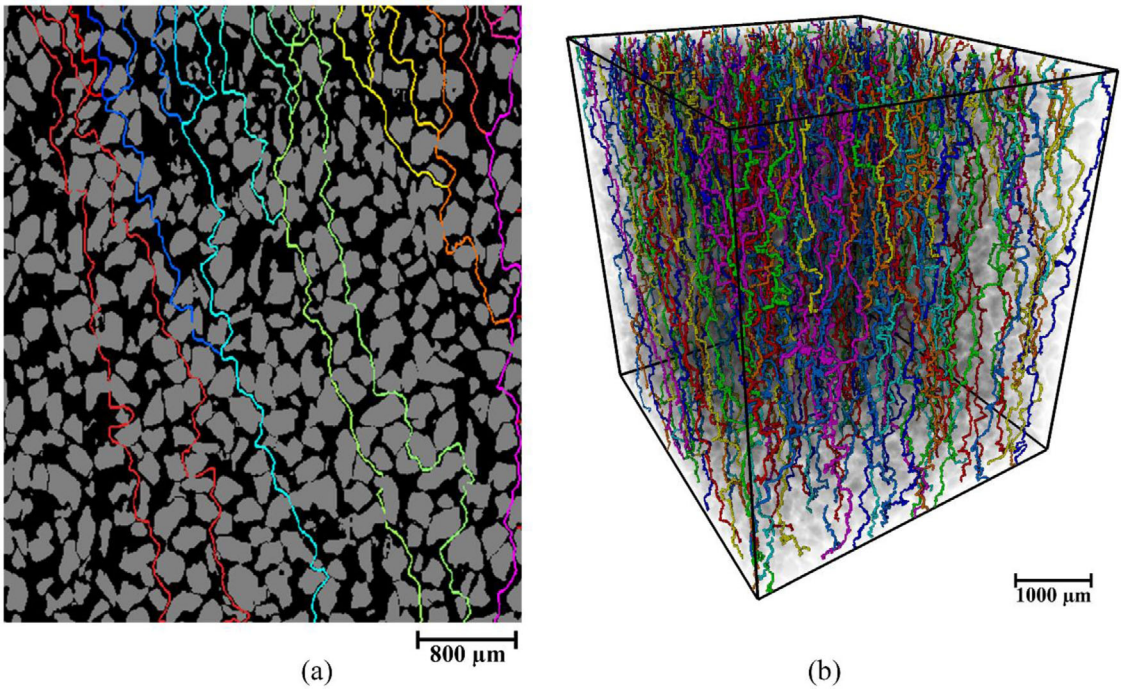

FIGURE 6 All possible connected paths in (a) two-dimensional image (flow from top to bottom of the image) where gray color represents sand particles and black color represents the void space; and (b) three-dimensional image (flow from top to bottom of the image)

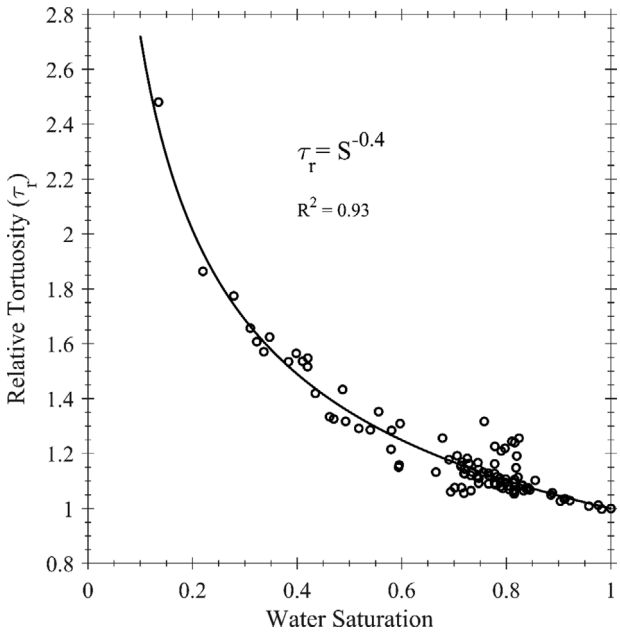

FIGURE 7 Change of relative tortuosity with degree of saturation for the 130 systems

the use of a monochromator reduces the flux significantly, transmitting only 0.1% of the beam energy, which increases data acquisition time and makes it unsuitable for monitoring dynamic processes (Rivers, 2016). An alternative is the use of pink beam technique (SMT-P) where the monochromator is replaced with a grazing mirror and X-ray absorbing foil. The SMT-P technique can yield an X-ray flux three orders of magnitude higher than SMT-M, reducing the data acquisition time to few seconds and makes a favorable option for in situ monitoring of dynamic processes (Jarrar, Alshibli, et al., 2020; Rivers, 2016). In this study, both SMT-M and SMT-P techniques were used to acquire 3D images of unconsolidated porous media systems at different degrees of the wetting phase saturation. All scans were acquired at Beamline 13D of the Advanced Photon Source (APS), Argonne National Laboratory (ANL), Illinois, USA.

2.2 | Materials and experimental method

The porous media used in this study was silica sand obtained from two suppliers: US Silica Company and Agsco. An aluminum cylindrical cell with an inner diameter of 6.35 mm (1/4 inch) and a height of 38.1 mm (1.5 inches) was used for the flow experiments. The flow cell has two ports: an upper port connected to a DigiFlow pressure-volume actuator (flow pump), and a bottom port connected to a pressure regulator connected to a CO_2 gas source (Figure 1). Sand was deposited into the partially filled with water cell to achieve an initial fully saturated state. During experiments, water (wetting phase) was pumped out of the cell through the top port at a flow rate of 0.01 ml min^{-1} while injecting CO_2 (nonwetting phase) through the bottom port at a constant pressure of 20.7 kPa (3 psi).

TABLE 3 Results of the nonlinear regression model for geometric tortuosity

Model: $\tau = \phi^{\beta_1} S^{\beta_2} C_c^{\beta_3} I_R^{\beta_4}$			
Coefficient	**Estimate**	**Standard error**	***p* value**
β_1	−0.35	0.0140	<.01
β_2	−0.4	0.0148	<.01
β_3	0.5	0.1253	<.01
β_4	−0.5	0.0531	<.01

Note. τ, tortuosity; ϕ, porosity; *S*, water saturation; C_c, coefficient of curvature; I_R, roundness index.

Full 3D tomography scans were acquired continuously using SMT-P (83 systems) and SMT-M (47 systems). A total of 130 porous media systems with wide ranges of degree of saturation (S), porosity (ϕ), roundness (I_R), sphericity (I_{sph}), mean grain diameter (d_{50}), and grain size distribution were imaged and analyzed in this study (Table 2). The degree of wetting phase saturation ranged from 13.5 to 100%; porosity ranged from 0.30 to 0.50; and d_{50} ranged from 370 to 960 μm. Moreover, histograms of porosity, d_{50}, I_R, I_{sph}, C_u, C_c, pore radius, and throat radius of the 130 systems are depicted in Figure 2. The 3D images had three different sizes: 1,920 × 1,920 × 1,200 voxels with a spatial resolution of 4.29 μm voxel^{-1} (83 datasets), 550 × 550 × 520 voxels with a spatial resolution of 11.22 μm voxel^{-1} (13 datasets), and 400 × 400 × 400 voxels with a spatial resolution of 11.22 μm voxel^{-1} (34 datasets). A total of 27 unique samples of unconsolidated sand packs, which broadly varies in grain sizes, were organized in three different physical sizes and correspondingly different imaging resolutions. To obtain different degrees of wetting phase saturations, a given sand pack was scanned at 100% saturation and then gradually drained and scanned at each drainage step for the corresponding degree of saturation. A 3D image from a scan represent a single "system," at a specific saturation level, for a specific sample of unconsolidated sand pack.

3 | RESULTS AND DISCUSSION

3.1 | Sand particles segmentation

PerGeos software (FEI, 2019) was used to analyze 3D images including image enhancement and segmentation. Figure 3 summaries the image processing steps for a zoomed view of an XY slice of one of the systems. First, a combination of anisotropic diffusion and median filters were used to reduce noise in the grayscale SMT images and enhance their contrast. The anisotropic diffusion filter compares the value of each voxel with its six neighboring voxels and diffuses the voxel if the difference is smaller than the diffusion stop threshold value. The resulting image is a smoothed grayscale image with sharp particle edges (Figure 3b). The next step is to segment the filtered image to separate sand particles from the surrounding wetting and nonwetting phases (Figure 3c).

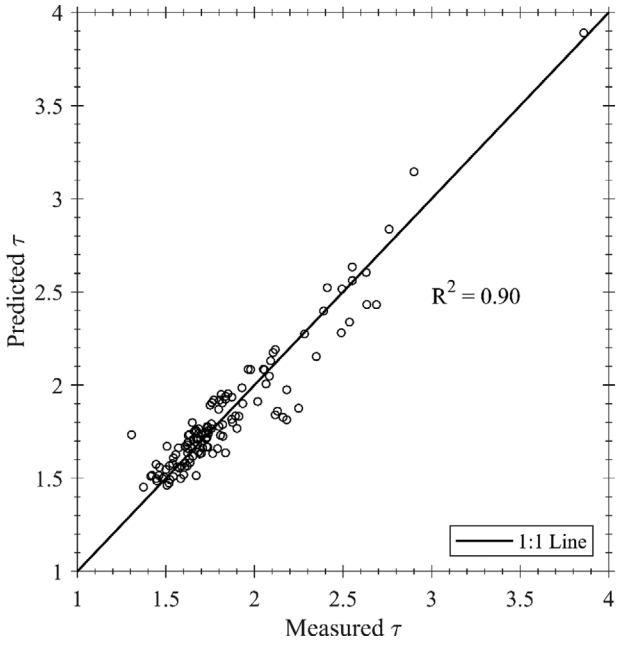

FIGURE 8 Measured geometric tortuosity (τ) from synchrotron microcomputed tomography (SMT) images vs. predicted geometric τ estimated from Equation 15

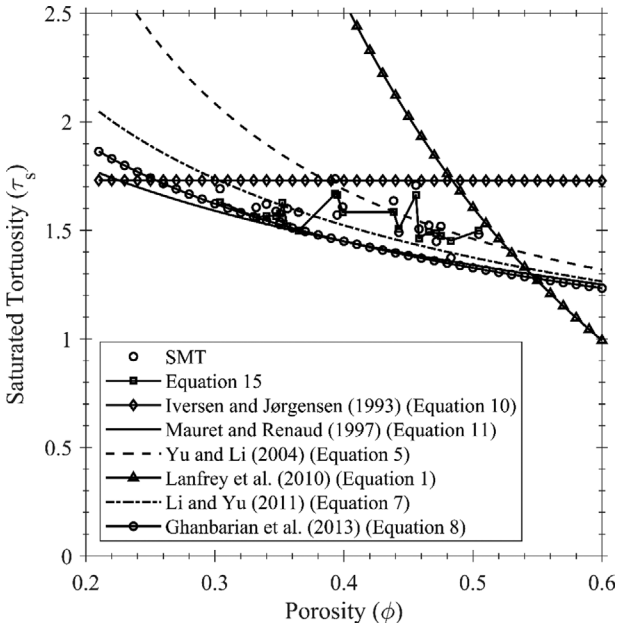

FIGURE 9 Comparison of the predicted saturated geometric tortuosity using the model in Equation 15 with analytical and theoretical models from the literature. SMT, synchrotron microcomputed tomography

Filtered images were binarized using an interactive thresholding module where user-defined values of image intensity ranges were used to binarize the images. The thresholding range was selected based on intensity histograms of

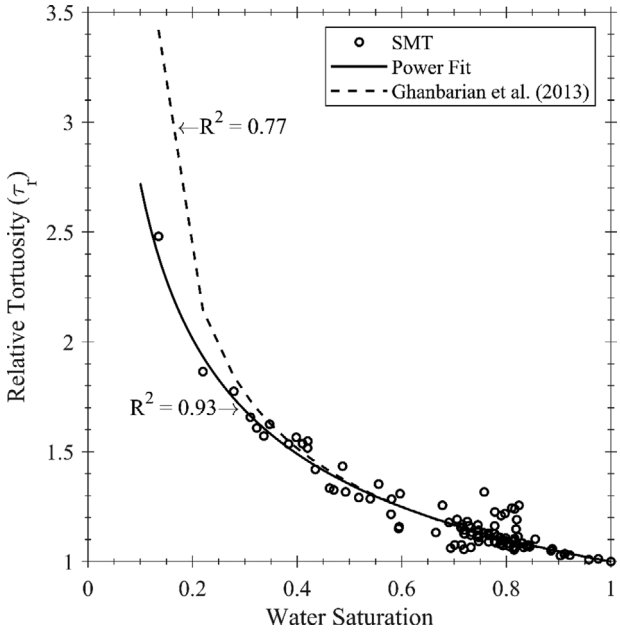

FIGURE 10 Comparison of the predicted relative tortuosity using the model in Equation 14 with the model proposed by Ghanbarian, Hunt, Sahimi, et al. (2013). SMT, synchrotron microcomputed tomography

the images and was verified visually for accuracy before proceeding with the segmentation (Al-Raoush, 2012; Jarrar, Al-Raoush, et al., 2020). Then, the Separate Objects module in PerGeos software was used to identify individual sand particles where each particle was assigned a unique numerical label (Figure 3d, e). The Separate Objects module is a combination of watershed, distance transform, and numerical reconstruction algorithms that accurately remove small areas of contact between particles. Figure 4 shows 2D cross-section and volume rendering snapshots for selected labeled images where each labeled particle consists of connected voxels occupying a cubical point in 3D space. Labeled sand images were then used to compute the porosity of a given system as the ratio of the volume of voids to the total volume. The accuracy of the segmentation of the void and solid phases was verified by comparing porosity values obtained from segmented images with values obtained from direct measurement of porosity. Columns were initially fully saturated with water and then carefully packed with sand samples. The weight of each column before and after packing was recorded to obtain the volume of void space required to measure porosity of each sand sample. The volume of each particle was computed as the summation of all voxels within the particle.

3.2 | Segmentation of wetting and nonwetting phases

Similar to sand particles segmentation, the filtered images were used to segment the nonwetting phase (CO_2) using the interactive thresholding module. The thresholding range was selected based on the images histograms and was checked visually for accuracy. Finally, arithmetic operations were performed on the binarized sand and nonwetting phase images to yield one segmented image with all three phases of solids, wetting (water), and nonwetting with each phase having a distinct value (i.e., solid particles have a value of 3, wetting phase has a value of 2, and nonwetting phase has a value of 1, Figure 3g). Figure 5 depicts a volume rendering snapshot for a sample three-phase segmented image. The three-phase segmented images were used to compute the degree of saturation as the volume of the wetting phase divided by the total volume of voids (wetting phase + nonwetting phase) of all systems.

3.3 | Particle morphology and gradation

Two morphology indices were adopted to quantify the morphology of sand particles: roundness (I_R), and sphericity (I_{sph}) indices. Alshibli et al. (2015) proposed a definition of I_{sph} based on 3D SMT images as

$$I_{sph} = \frac{V_p}{V_s} \tag{13}$$

where V_s is the volume of a sphere with a diameter equal to the shortest length that passes through the centroid of the particle. In this study, the definition proposed by Lanfrey et al. (2010) (Equation 2) is used to compute I_R, whereas the definition proposed by Alshibli et al. (2015) (Equation 13) is used to calculate I_{sph}. Uniformity coefficient ($C_u = d_{60}/d_{10}$), and coefficient of curvature [$C_c = d_{30}^2/(d_{10}d_{60})$] are used to describe the grain size distribution of the porous media systems where d_{10}, d_{30}, and d_{60} are the diameters corresponding to 10, 30, and 60% finer in the particle-size distribution, respectively.

Longest and shortest diameters measurements needed for the morphology indices and gradation coefficients were obtained by calculating the 3D Ferret diameter of all sand particles. Feret diameter is defined as the distance between two parallel tangent planes of a particle at a given direction (like measurements by a caliper). The 3D Feret diameters were calculated for each sand particle with a sampling of 60 angles regularly spread around the upper part of a unit sphere, which can determine the maximum (longest) and minimum (shortest) diameter of each sand particle.

3.4 | Geometric tortuosity results

Binarized images, where wetting phase voxels have values of 1 and nonwetting phase and sand voxels have values of 0, were then used to compute the geometric tortuosity for the

TABLE 4 Assumptions and parameters used to predict tortuosity for the models in Figure 9

Equation	Assumptions	Reference
1	I_R was assumed to be the mean value of all experimental systems	Lanfrey et al. (2010)
5	No assumptions	Yu and Li (2004)
7	No assumptions	Li and Yu (2011)
8	$\theta_t = 0.1\phi$ (per Hunt, 2004) $\nu = 0.88$ (three-dimensional flow) $D_x = 1.43$ (fractal dimensionality of the optimal paths in three dimension) $C \ll L_S$ $(\frac{C}{L_S}) = 0$	Ghanbarian, Hunt, Sahimi, et al. (2013)
10	No assumptions	Iversen and Jørgensen (1993)
11	No assumptions ($p = .49$)	Mauret and Renaud (1997)

Note. I_R, roundness index; θ_t, critical volumetric water content for percolation; ϕ, porosity; ν, scaling factor; D_x, fractal dimensionality; C, numerical fitting factor; L_S, system size.

wetting phase using the tortuosity module in PerGeos software. The module computes the tortuosity of a path formed by the centroids on each plane along the z axis of the binarized 3D image by computing the path length through the centroids divided by the number of planes along the z axis (FEI, 2018). Figure 6a depicts a sample 2D slice obtained from a 3D image to visualize the connected paths in the porous media in 2D, which shows that all tortuous paths were accurately identified in the direction of flow (top to bottom of the image). Similarly, Figure 6b shows all connected paths in a sample 3D image when the direction of flow from top to bottom of the image.

Figure 7 presents the change of relative tortuosity with wetting phase saturation for the 130 sand systems along with the best power fit (depicted as solid line), which is found to be

$$\tau_r = \frac{\tau}{\tau_s} = S^{-0.4} \tag{14}$$

The power function of wetting phase saturation (Equation 14) provides a good estimate of the relative tortuosity with an R^2 value of .93 even with the variation of porosity in the sand systems for the porosity range of the natural unconsolidated porous media systems investigated here. Furthermore, the minimum allowable value of τ_r according to Equation 14 is 1.0 and is reached when $S = 1.0$, which is in agreement with the definition of τ_r. The power function in (Equation 14) uses the form proposed by (Mualem, 1976), which has an exponent of −0.5; the 130 saturations from the tomography images revealed that an exponent of −0.4 gives a better fit for variably saturated unconsolidated porous media. It is to be noted that removing the data point at lowest saturation in Figure 7 gives an R^2 value of .91. Moreover, 10-fold cross validation was conducted with 80% of the dataset to train the model and 20% for testing, the test portion of the model had an average R^2 of .92 and RMSE of 0.05.

Multivariate nonlinear regression was used to generate a model that predicts geometric tortuosity of saturated and unsaturated porous media using S, ϕ, D_{50}, I_{sph}, I_R, C_u, and C_c as possible predictors. Regression coefficients were determined based on the least square fit which minimizes the sum of the squares of the residuals. The p value was used to assess the significance of each regression coefficient. A coefficient with a low p value means that the null hypothesis that the coefficient is equal to zero can be rejected. Only variables with a p value less than .05 are kept in the model. The regression yielded the following model:

$$\tau = \phi^{-0.35} S^{-0.4} \sqrt{\frac{C_c}{I_R}} \tag{15}$$

with a RMSE of 0.117 and an R^2 value of .90. Effects of I_{sph} and C_u were found to be insignificant based on their p value and were excluded from the regression model. Table 3 lists the nonlinear regression coefficients along with their standard errors and corresponding p values and Figure 8 displays the measured geometric tortuosity obtained from SMT images vs. the predicted geometric tortuosity estimated from Equation 15 along with 1:1 line. I_{sph} and C_u were excluded from the regression model because the corresponding p value of these two predictors was larger than the .05 threshold. In other words, changing the power coefficient of the two predictors did not change the response of the model, and therefore, their effects were negligible.

Although Equation 14 determines the relative geometric tortuosity as a function of wetting phase saturation, Equation 15 determines geometric tortuosity as a function of porosity and sand characteristics. Moreover, 10-fold cross validation was conducted with 80% of the dataset to train the model and 20% for testing, the test portion of the model had an average R^2 of .89 and RMSE of 0.12. MATLAB software was used to perform the multivariate nonlinear regression, the 10-fold cross validation and to determine the fit of the presented models. The significance of I_R and C_c agree with finding of (Zhang, 2020), reflecting influence of particle arrangement on tortuosity.

Figure 9 compares the predicted saturated geometric tortuosity calculated using the model proposed in Equation 15 with analytical, theoretical, and empirical models obtained

from the literature. Referring to Figure 9, Mauret and Renaud (1997) and Ghanbarian, Hunt, Sahimi, et al. (2013) models underestimate the geometric tortuosity values while Iversen and Jørgensen (1993) and Lanfrey et al. (2010) models overestimate tortuosity for the porosity range reported in this study. It should be noted that for Ghanbarian, Hunt, Sahimi, et al. (2013) model, θ_t was approximated to be 0.1ϕ (Hunt, 2004), and finite-size effect was neglected. Yu and Li (2004) model overlaps with the proposed statistical fit model (Equation 15) at porosity value of 0.45 but began to diverge and overestimate the tortuosity as porosity decreased. Li and Yu (2011) model shows good agreement with the statistical fit model defined by Equation 15, but starts to diverge for porosity values less than 0.30. Table 4 lists all the assumptions and parameters used to plot the predictive tortuosity models on Figure 9, the mean I_R of the 130 experimental systems is equal to 0.78. Figure 10 presents a comparison of the predicted relative geometric tortuosity using the statistical fit model in Equation 14 with the model proposed by Ghanbarian, Hunt, Sahimi, et al. (2013) that was derived based on percolation theory. For Figure 10, θ_t was approximated to be 0.1ϕ based on the porosity measurements from the dataset, the finite-size effect was neglected, and the 3D values of the fractal dimensionality of the optimal path and the scaling component ν were used (1.43 and 0.88, respectively). It can be seen from Figure 10 that the model that was generated based on percolation theory is in good agreement with the statistical fit model (Equation 14) with an R^2 value of .77. The model began to slightly diverge at degrees of saturation less than 0.25.

4 | CONCLUSIONS

Multivariate nonlinear regression fitting was used to propose a geometric tortuosity model for saturated and unsaturated porous media based on in situ 3D images of unconsolidated sand systems. Full 3D tomography images of 130 natural sand systems with a range of porosity, saturation, grain size distribution, and morphology were acquired using SMT-M and dynamic SMT-P imaging techniques. The degree of saturation of the sand systems ranged from 13.5 to 100%, whereas the porosity ranged from 0.30 to 0.50. All images were segmented and analyzed, and the geometric tortuosity of each system was determined using PerGeos commercial software.

Even with the variation of porosity in the sand systems, the relative tortuosity can be estimated as a power function of saturation only with an R^2 value of .93. This is only true for the porosity range investigated in this study (0.30–0.50). Multivariate nonlinear regression was used to propose a model that estimates geometric tortuosity of saturated and unsaturated porous media with S, ϕ, D_{50}, I_{sph}, I_R, C_u, and C_c as possible predictors. Effects of I_{sph} and C_u were found to be insignificant based on their p value and were excluded from the regression model. The proposed model provided a good estimate of geometric tortuosity with an R^2 value of .90 and RMSE value of 0.117. The proposed model yields better estimates of saturated geometric tortuosity compared with the analytical and theoretical models currently reported in the literature, which can be attributed to the fact that these models were developed for ideal systems with assumptions that might not be representative of natural porous media.

ACKNOWLEDGMENTS

Open Access funding provided by the Qatar National Library. This publication was made possible by funding from Grant no. NPRP8-594-2-244 from the Qatar national research fund (a member of Qatar Foundation) and the Institute for a Secure and Sustainable Environment (ISSE), University of Tennessee-Knoxville, USA. Any opinions, findings, and conclusions or recommendations expressed in this material are those of the authors and do not necessarily reflect the views of funding agencies. The authors would like to thank Mr. Wadi Imseeh for his help during scanning. This paper used resources of the Advanced Photon Source (APS), a USDOE Office of Science User Facility operated for the USDOE Office of Science by Argonne National Laboratory (ANL) under Contract no. DE-AC02-06CH11357. The PSMT images presented in this paper were collected using the X-ray Operations and Research Beamline Station 13-BMD at Argonne Photon Source (APS), ANL. We thank Dr. Mark Rivers of APS for help in performing the SMT scans. We also acknowledge the support of GeoSoilEnviroCARS (Sector 13), which is supported by the National Science Foundation, Earth Sciences (EAR-1128799), and the USDOE, Geosciences (DE-FG02-94ER14466). The authors would also like to thank the anonymous reviewers who contributed with comments and suggestions to improve this paper.

AUTHOR CONTRIBUTIONS

Zaher A. Jarrar: Conceptualization, Methodology, Software, Formal analysis, Original draft preparation. Riyadh I Al-Raoush: Conceptualization; Formal analysis; Funding acquisition; Investigation; Methodology; Project administration; Resources; Supervision; Writing-review & editing. Jamal A. Hunnun: Methodology, Software, Formal analysis, Writing-Reviewing and Editing, Khalid A. Alshibli: Conceptualization; Funding acquisition; Investigation; Methodology; Resources; Supervision; Writing-review & editing.

CONFLICT OF INTEREST

The authors declare no conflict of interest.

ORCID

Riyadh I. Al-Raoush https://orcid.org/0000-0001-9420-014X

REFERENCES

Ahmadi, M. M., Mohammadi, S., & Hayati, A. N. (2011). Analytical derivation of tortuosity and permeability of monosized spheres: A volume averaging approach. *Physical Review E*, *83*(2), 026312. https://doi.org/10.1103/PhysRevE.83.026312

Al-Raoush, R. (2012). Change in microstructure parameters of porous media over representative elementary volume for porosity. *Particulate Science and Technology*, *30*(1), 1–16. https://doi.org/10.1080/02726351.2010.543262

Al-Raoush, R. I., & Madhoun, I. T. (2017). TORT3D: A MATLAB code to compute geometric tortuosity from 3D images of unconsolidated porous media. *Powder Technology*, *320*, 99–107. https://doi.org/10.1016/j.powtec.2017.06.066

Alshibli, K. A., Druckrey, A. M., Al-Raoush, R. I., Weiskittel, T., & Lavrik, N. V. (2015). Quantifying morphology of sands using 3D Imaging. *Journal of Materials in Civil Engineering*, *27*(10), 04014275. https://doi.org/10.1061/(ASCE)MT.1943-5533.0001246

Androutsopoulos, G. P., & Salmas, C. E. (2000). Tomography of macro-meso-pore structure based on mercury porosimetry hysteresis. *Chemical Engineering Communications*, *181*(1), 137–177. https://doi.org/10.1080/00986440008912819

Clennell, M. B. (1997). Tortuosity: A guide through the maze. *Geological Society, London, Special Publications*, *122*(1), 299. https://doi.org/10.1144/GSL.SP.1997.122.01.18

Comiti, J., & Renaud, M. (1989). A new model for determining mean structure parameters of fixed beds from pressure drop measurements: Application to beds packed with parallelepipedal particles. *Chemical Engineering Science*, *44*(7), 1539–1545. https://doi.org/10.1016/0009-2509(89)80031-4

Corrochano, B. R., Melrose, J. R., Bentley, A. C., Fryer, P. J., & Bakalis, S. (2015). A new methodology to estimate the steady-state permeability of roast and ground coffee in packed beds. *Journal of Food Engineering*, *150*, 106–116. https://doi.org/10.1016/j.jfoodeng.2014.11.006

Du Plessis, J. P., & Masliyah, J. H. (1991). Flow through isotropic granular porous media. *Transport in Porous Media*, *6*(3), 207–221. https://doi.org/10.1007/BF00208950

Duda, A., Koza, Z., & Matyka, M. (2011). Hydraulic tortuosity in arbitrary porous media flow. *Physical Review E*, *84*(3), 036319. https://doi.org/10.1103/PhysRevE.84.036319

Epstein, N. (1989). On tortuosity and the tortuosity factor in flow and diffusion through porous media. *Chemical Engineering Science*, *44*(3), 777–779. https://doi.org/10.1016/0009-2509(89)85053-5

FEI. (2018). Avizo. Version 9.7. FEI.

FEI. (2019). PerGeos. Version 2019. FEI.

Gao, X., da Costa, D., & Bhatia, S. K. (2014). Understanding the diffusional tortuosity of porous materials: An effective medium theory perspective. *Chemical Engineering Science*, *110*, 55–71. https://doi.org/10.1016/j.ces.2013.09.050

Garrouch, A. A., Ali, L., & Qasem, F. (2001). Using diffusion and electrical measurements to assess tortuosity of porous media. *Industrial & Engineering Chemistry Research*, *40*(20), 4363–4369. https://doi.org/10.1021/ie010070u

Ghanbarian, B., Hunt, A. G., Ewing, R. P., & Sahimi, M. (2013). Tortuosity in porous media: A critical review. *Soil Science Society of America Journal*, *77*(5), 1461–1477. https://doi.org/10.2136/sssaj2012.0435

Ghanbarian, B., Hunt, A. G., Sahimi, M., Ewing, R. P., & Skinner, T. E. (2013). Percolation theory generates a physically based description of tortuosity in saturated and unsaturated porous media. *Soil Science Society of America Journal*, *77*(6), 1920–1929. https://doi.org/10.2136/sssaj2013.01.0089

Grathwohl, P. (2012). *Diffusion in natural porous media: Contaminant transport, sorption/desorption and dissolution kinetics* (Vol. 1). Springer Science & Business Media.

Hunt, A. G. (2004). Continuum percolation theory for water retention and hydraulic conductivity of fractal soils: Estimation of the critical volume fraction for percolation. *Advances in Water Resources*, *27*(2), 175–183. https://doi.org/10.1016/j.advwatres.2003.10.004

Iversen, N., & Jørgensen, B. B. (1993). Diffusion coefficients of sulfate and methane in marine sediments: Influence of porosity. *Geochimica et Cosmochimica Acta*, *57*(3), 571–578. https://doi.org/10.1016/0016-7037(93)90368-7

Jarrar, Z. A., Al-Raoush, R. I., Hannun, J. A., Alshibli, K. A., & Jung, J. (2020). 3D synchrotron computed tomography study on the influence of fines on gas driven fractures in sandy sediments. *Geomechanics for Energy and the Environment*, *23*, 100105. https://doi.org/10.1016/j.gete.2018.11.001

Jarrar, Z. A., Alshibli, K. A., Al-Raoush, R. I., & Jung, J. (2020). 3D measurements of hydrate surface area during hydrate dissociation in porous media using dynamic 3D imaging. *Fuel*, *265*, 116978. https://doi.org/10.1016/j.fuel.2019.116978

Jung, J., Hamachi, M., Obara, Y., Tanikura, I., & Watanabe, S. (2014). *Analysis of damage in specimen under cyclic uniaxial loading test by X-ray CT method* [Paper ISRM-ARMS8-2014-040]. ISRM International 8th Asian Rock Mechanics Symposium, Sapporo, Japan.

Kinney, J. H., & Nichols, M. C. (1992). X-ray tomographic microscopy (XTM) using synchrotron radiation. *Annual review of Materials Science*, *22*(1), 121–152. https://doi.org/10.1146/annurev.ms.22.080192.001005

Lanfrey, P.-Y., Kuzeljevic, Z. V., & Dudukovic, M. P. (2010). Tortuosity model for fixed beds randomly packed with identical particles. *Chemical Engineering Science*, *65*(5), 1891–1896. https://doi.org/10.1016/j.ces.2009.11.011

Li, A., & Payandeh, S. (2016). *An overview of path tortuosity measures for tracking and monitoring* [Paper presentation]. 2016 IEEE 7th Annual Information Technology, Electronics and Mobile Communication Conference (IEMCON). https://doi.org/10.1109/IEMCON.2016.7746271

Li, J.-H. & Yu, B.-M. (2011). Tortuosity of flow paths through a Sierpinski carpet. *Chinese Physics Letters*, *28*(3), 034701. https://doi.org/10.1088/0256-307X/28/3/034701

Mauret, E., & Renaud, M. (1997). Transport phenomena in multi-particle systems: I. Limits of applicability of capillary model in high voidage beds-application to fixed beds of fibers and fluidized beds of spheres. *Chemical Engineering Science*, *52*(11), 1807–1817. https://doi.org/10.1016/S0009-2509(96)00499-X

Morin, R. H., Leblanc, D. R., & Troutman, B. M. (2010). The influence of topology on hydraulic conductivity in a sand-and-gravel aquifer. *Groundwater*, *48*(2), 181–190. https://doi.org/10.1111/j.1745-6584.2009.00646.x

Mualem, Y. (1976). A new model for predicting the hydraulic conductivity of unsaturated porous media. *Water Resources Research*, *12*(3), 513–522. https://doi.org/10.1029/WR012i003p00513

Naveed, M., Hamamoto, S., Kawamoto, K., Sakaki, T., Takahashi, M., Komatsu, T., Moldrup, P., Lamandé, M., Wildenschild, D., Prodanović, M., & De Jonge, L. W. (2013). Correlating gas transport parameters and X-ray computed tomography measurements

in porous media. *Soil Science*, *178*(2). https://doi.org/10.1097/SS.0b013e318288784c

Neethirajan, S., Jayas, D. S., White, N. D. G., & Zhang, H. (2008). Investigation of 3D geometry of bulk wheat and pea pores using X-ray computed tomography images. *Computers and Electronics in Agriculture*, *63*(2), 104–111. https://doi.org/10.1016/j.compag.2008.01.019

Pardo-Alonso, S., Vicente, J., Solórzano, E., Rodriguez-Perez, M. Á., & Lehmhus, D. (2014). Geometrical tortuosity 3D calculations in infiltrated aluminium cellular materials. *Procedia Materials Science*, *4*, 145–150. https://doi.org/10.1016/j.mspro.2014.07.553

Pisani, L. (2011). Simple expression for the tortuosity of porous media. *Transport in Porous Media*, *88*(2), 193–203. https://doi.org/10.1007/s11242-011-9734-9

Promentilla, M., Cortez, S., Papel, R., Tablada, B., & Sugiyama, T. (2016). Evaluation of microstructure and transport properties of deteriorated cementitious materials from their X-ray computed tomography (CT) images. *Materials*, *9*(5), 388. https://doi.org/10.3390/ma9050388

Qin, X., Cai, J., Xu, P., Dai, S., & Gan, Q. (2019). A fractal model of effective thermal conductivity for porous media with various liquid saturation. *International Journal of Heat and Mass Transfer*, *128*, 1149–1156. https://doi.org/10.1016/j.ijheatmasstransfer.2018.09.072

Rivers, M. L. (2016). *High-speed tomography using pink beam at GeoSoilEnviroCARS* (Vol. 9967). SPIE. https://doi.org/10.1117/12.2238240

Rotger, D., Rosales, M., Garcia, J., Pujol, O., Mauri, J., & Radeva, P. (2003). ActiveVessel: a new multimedia workstation for intravascular ultrasound and angiography fusion. *Computers in Cardiology*, *30*, 65–68.

Salmas, C. E., & Androutsopoulos, G. P. (2001). A novel pore structure tortuosity concept based on nitrogen sorption hysteresis data. *Industrial & Engineering Chemistry Research*, *40*(2), 721–730. https://doi.org/10.1021/ie000626y

Soukup, K., Hejtmánek, V., Čapek, P., Stanczyk, K., & Šolcová, O. (2015). Modeling of contaminant migration through porous media after underground coal gasification in shallow coal seam. *Fuel Processing Technology*, *140*, 188–197. https://doi.org/10.1016/j.fuproc.2015.08.033

Takahashi, H., Seida, Y., & Yui, M. (2009). 3D X-ray CT and diffusion measurements to assess tortuosity and constrictivity in a sedimentary rock. *Diffus Fundam*, *11*, 1–11.

Takahashi, M., Takada, N., Sato, M., & Lin, W. (2015). *Three dimensional pore geometry and fluid flow of Kimachi sandstone under different stress condition: Suggestion to conservation of tuffacious world cultural heritage*. Engineering Geology for Society and Territory.

Vervoort, R. W., & Cattle, S. R. (2003). Linking hydraulic conductivity and tortuosity parameters to pore space geometry and pore-size distribution. *Journal of Hydrology*, *272*(1), 36–49. https://doi.org/10.1016/S0022-1694(02)00253-6

Weerts, A. H., Kandhai, D., Bouten, W., & Sloot, P. M. A. (2001). Tortuosity of an unsaturated sandy soil estimated using gas diffusion and bulk soil electrical conductivity. *Soil Science Society of America Journal*, *65*(6), 1577–1584. https://doi.org/10.2136/sssaj2001.1577

Wong, P.-Z. (1999). Conductivity, permeability, and electrokinetics. In P.-Z. Wong (Ed.), *Experimental methods in the physical sciences* (Vol. 35, pp. 119–159). Academic Press. https://doi.org/10.1016/S0076-695X(08)60415-9

Xu, W., Jia, M., & Gong, Z. (2018). Thermal conductivity and tortuosity of porous composites considering percolation of porous network: From spherical to polyhedral pores. *Composites Science and Technology*, *167*, 134–140. https://doi.org/10.1016/j.compscitech.2018.07.038

Yu, B.-M., & Li, J.-H. (2004). A geometry model for tortuosity of flow path in porous media. *Chinese Physics Letters*, *21*(8), 1569–1571. https://doi.org/10.1088/0256-307X/21/8/044

Zhang, Z. F. (2020). Algebraic expressions for estimating the impact depths of a surface barrier over a homogeneous soil. *Vadose Zone Journal*, *19*(1), e20003. https://doi.org/10.1002/vzj2.20003

Zielinski, T. G. (2012). *Inverse identification and microscopic estimation of parameters for models of sound absorption in porous ceramics*. In *Proceedings of ISMA2012-USD2012* pp. 95–108). Katholieke Universiteit Leuven.

How to cite this article: Jarrar ZA, Al-Raoush RI, Hannun JA, Alshibli KA. New model for estimating geometric tortuosity of variably-saturated porous media using 3D synchrotron microcomputed tomography imaging. *Soil Sci Soc Am J*, 2021;*85:*1867–1879. https://doi.org/10.1002/saj2.20289